

Chapter 12

Normal Phase of Polarised Strongly Interacting Fermi Gases

Alessio Recati and Sandro Stringari

Abstract The theory of the normal phase of strongly interacting polarized atomic Fermi gases at zero temperature is reviewed. We use the formalism of quasi-particles to build up the equation of state of the normal phase with the relevant parameters calculated via Monte-Carlo. The theory is used to discuss the phase diagram of polarized Fermi gases at unitarity. The Fermi liquid nature of these configurations is pointed out. The theory provides accurate predictions for many different quantities experimentally measured, like the Chandrasekhar–Clogston limit of critical polarization, the density profiles and the Radio-Frequency spectrum.

12.1 Introduction

The observation of superfluidity in ultra-cold Fermi gases has built a new bridge between the field of atomic gases and condensed matter. Moreover the flexibility one has in cold gases gives the possibility to explore new regimes and investigate new phases [1–3]. Remarkably in cold gases it is also possible to change the strength of the interatomic force between atoms. Due to the very low temperature and the diluteness of the gas the interaction can be described as a contact potential with strength $g = 4\pi\hbar^2 a/m$ where m is the mass of the atoms and a the scattering length. The latter depending on the atomic species can be changed by applying an external magnetic field profiting of the so-called Fano-Feshbach resonances (see e.g., [2], the article by Ketterle and Zwierlein in [1] and reference therein). Such a knob is one of

A. Recati (✉) · S. Stringari
Dipartimento di Fisica,
Università di Trento and CNR-INO BEC Center,
Povo 38121, Trento Italy
e-mail: recati@science.unitn.it

S. Stringari
e-mail: stringar@science.unitn.it

the key feature in the recent development of the field of cold gases and in particular has allowed to experimentally confirm the existence of a smooth crossover between the so-called Bardeen–Cooper–Schrieffer (BCS) regime of weakly attractive fermions and the Bose–Einstein condensation (BEC) of deeply bound pairs. The idea of a crossover, rather than a phase transition, was proposed in the early 80s by Leggett [4], Nozières and Schmitt-Rink [5].

While at $T = 0$ the state of a spin-1/2 Fermi gas with attractive interaction is a superfluid, a very interesting issue is what happens in the presence of spin population imbalance. In the standard BCS theory, superconductivity arises from Cooper pairing of opposite spin fermions, and is therefore sensitive to a mismatch between the Fermi surfaces of the two spin species. Indeed in a superconducting metal when we apply a magnetic field the coupling to the orbital motion (responsible for the Meissner effect) is negligible and the important effect is the coupling to the electron spins. The field can lower the energy of the spin-polarized normal state and, if it is strong enough, make the normal state energetically more favourable than the superconducting spin-singlet state. The value of the field at which this transition takes place is known as the Chandrasekhar–Clogston (CC) limit [6, 7] and, in a BCS superconductor, it requires that the field (or, in neutral systems, the chemical potential difference between the two spin states) be larger than $\Delta/\sqrt{2}$ where Δ is the superconductor gap. Crucially, this estimate assumes that the change in energy of the normal state due to polarization is only kinetic in origin and neglects changes in the interaction energy. However, if the system is strongly interacting, the value of the Chandrasekhar–Clogston field can also depend on the interactions in the normal state, an effect that must be accurately taken into account if we wish to study normal/superfluid coexistence.

Experimentally, the phase diagram of a polarized Fermi gas remained unexplored until recent work at MIT [8–10], Rice University [11, 12] and ENS [13–15] on ultra-cold Fermi gases, where experiments in the strongly interacting unitary limit of two-component atomic Fermi gases have been carried out. Such gases can be polarised leading to a state most naturally described as phase separated between a normal and a superfluid component.

In what follows we review the Fermi liquid theory of the normal state which was first introduced in [16] and its building block the Fermi polaron, i.e., a single impurity in an otherwise non-interacting Fermi gas. The normal phase has received a number of quite stringent experimental test. Its predictions for the critical polarization (related to the CC limit), the detailed structure of the density profiles agree very well with the experimental data obtained at MIT and ENS. The calculated value of the polaron parameters also agree with the ones found in very recent experiments [15, 17].

The same theory provides explicit predictions for the frequencies of the spin excitations in the normal phase and experiments in this direction would provide a crucial test of the applicability of Landau theory to the dynamics of these strongly interacting normal Fermi gases. We discuss this issue briefly at the end of the review.

In this review we do not follow the historical development of the understanding of the phase diagram for strongly interacting imbalanced Fermi gases. We rather start with the single impurity problem, then we consider the equation of state (EoS) for

finite concentration and the resulting nature and properties of the superfluid/normal phase transition. When possible we make comparison with experiments.

12.2 The $N + 1$ or Polaron Problem

12.2.1 Homogeneous Case

In this section we consider the extreme polarised case of a single impurity interacting attractively with a bath of N non-interacting fermions. It is worth mentioning that such a problem is the simplest realisation of the moving impurity problem, and it bears a strong similarity with other old and notoriously difficult condensed matter problems, such as the Kondo problem, the x-ray singularity in metals [18], the mobility of ions [19] and ^4He atoms in ^3He [20].

For later purpose let us identify with \uparrow the atoms in the bath and with \downarrow the impurity atom. Pictorially the bath will dress the impurity. Since the interaction is attractive, the impurity \downarrow prefers staying in the bath, gaining an energy μ_\downarrow and acquires a renormalised mass m^* . Sometimes μ_\downarrow is also called in literature binding energy for the simple fact that it is negative. The dressed particle is called Fermi-polaron or simply polaron in analogy with solid state physics concepts used to describe electrons dressed by optical phonons, hence a bath of bosons.

For weak interaction one can easily calculate within perturbation theory the two relevant parameters μ_\downarrow and m^* . Introducing the Fermi momentum of the bath $k_F = (6\pi^2 n)^{1/3}$, with n the density of the bath, one finds to second order in $k_F a$ the expressions

$$\mu_\downarrow = E_F \left(\frac{4k_F a}{3\pi} + \frac{2(k_F a)^2}{\pi^2} \right) \quad (12.1)$$

$$m^* = m \left(1 + \frac{4}{3\pi^2} (k_F a)^2 \right), \quad (12.2)$$

where $E_F = \hbar^2 k_F^2 / (2m)$ is the Fermi energy. They are the analogue of the Galitskii correction for the energy and the effective mass for a balanced weakly interacting Fermi gas [21]. Usually it is not easy to do much better than this, but for the present problem the fact that we are dealing with a single impurity in a non-interacting fermionic bath allows to obtain reliable results till unitarity using a simple variational approach. The starting point is to write the simplest non-trivial variational many-body wave-function for such a system, namely the sum of a non-interacting system with single particle-hole excitations. The trial wave function $|\psi\rangle$ for a system of total momentum \mathbf{p} is the following momentum eigenstate [22, 23]

$$|\psi\rangle = \phi_0^p |\mathbf{p}\rangle_{\downarrow} |0\rangle_{\uparrow} + \sum_{\substack{k > k_F \\ q < k_F}} \phi_{\mathbf{q}\mathbf{k}}^p |\mathbf{p} + \mathbf{q} - \mathbf{k}\rangle_{\downarrow} c_{\mathbf{k}\uparrow}^{\dagger} c_{\mathbf{q}\uparrow} |0\rangle_{\uparrow} \quad (12.3)$$

where $c_{\mathbf{k}\uparrow}$ and $c_{\mathbf{k}\uparrow}^{\dagger}$ are annihilation and creation operators of atoms in the bath with momentum \mathbf{k} . In the first term the free Fermi sea is in its ground state $|0\rangle_{\uparrow} = \prod_{k < k_F} c_{\mathbf{k}\uparrow}^{\dagger} |v\rangle$ ($|v\rangle$ is the vacuum) and the impurity atom is in the plane-wave state $|\mathbf{p}\rangle_{\downarrow}$, while the second term is an excited state corresponding to the creation of a particle-hole pair in the Fermi sea with momentum \mathbf{k} and \mathbf{q} respectively and the \downarrow -spin atom carrying the rest of the momentum. The first part corresponds to free propagation and, thus, $|\phi_0^p|^2$ is to the quasi-particle residue Z_p [24]. The coefficients ϕ_0^p and $\phi_{\mathbf{q}\mathbf{k}}$ are found by minimizing the total energy. In the minimisation procedure one has to handle, as usual, with the zero range interaction potential and the corresponding regularisation in terms of the scattering length (see, e.g., [21]). In this way one gets for the energy change:

$$E = \epsilon_{\downarrow p} + \sum_{q < k_F} f(E, \mathbf{p}, \mathbf{q}) \quad (12.4)$$

$$\frac{1}{f(E, \mathbf{p}, \mathbf{q})} = \frac{m}{4\pi a} - \sum_k \frac{m}{k^2} + \sum_{k > k_F} \frac{1}{\epsilon_{\uparrow k} + \epsilon_{\downarrow \mathbf{p} + \mathbf{q} - \mathbf{k}} - \epsilon_{\uparrow q} - E}$$

where $\epsilon_{\uparrow, \downarrow k} = k^2/2m$ is the kinetic energy of the \uparrow and \downarrow atoms. For $\mathbf{p} = 0$ we have $E = \mu_{\downarrow}$, while the variation of E for small \mathbf{p} gives the effective mass. In Fig. 12.1 we report the results for the energy of the polaron as a function of the inverse of the interaction $1/k_F a$. In the same figure we report the perturbative result (12.2) as well as the results (Stefano Giorgini, private communication) obtained by using Fixed-Node Diffusion Monte-Carlo (FN-DMC) simulations. The latter technique is a zero-temperature Monte-Carlo technique based on a trial wave function which fixes the nodal surface, used as an ansatz in the DMC. We restrict the analysis to the case where there are no bound states between the \uparrow and the \downarrow atoms. Such a bound state clearly exists in the BEC limit $1/k_F a \rightarrow +\infty$, where molecules are present. While the present approach recovers this limiting behavior, the effect of a bound state in the intermediate regime has to be properly taken into account [25–27] and it is not well described by the variational ansatz (12.3). The point is that, as it was first shown in [28], the polaron is not the lowest energy state any more for $1/k_F a \leq 1$. At the many-body level this would imply that at $T = 0$ one has a BEC of molecule almost for any polarization of the system. It is worth noticing that moreover as soon as the molecules are formed the system prefers to phase separate in a BEC of molecule and an ideal Fermi gas [29]. Thus the study of the physics of the molecular state embedded in an ideal Fermi gas [25–27] is experimentally challenging.

Going back to the results at unitarity ($k_F a \rightarrow \infty$), as can be seen from Fig. 12.1, the impurity chemical potential approaches the value $\sim 3/5 E_F$ which means that the bath “dresses” the impurity with just a single atom. The effect on the mass is even

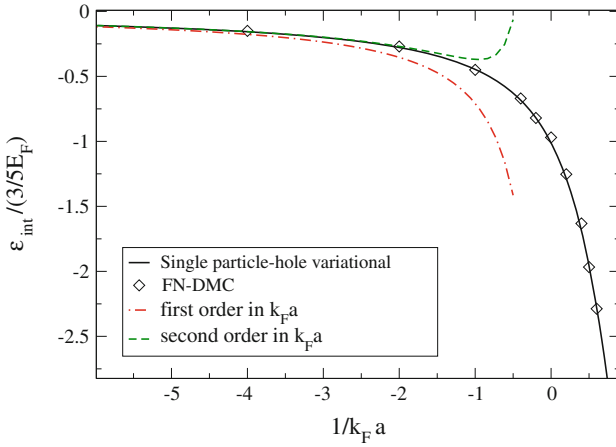


Fig. 12.1 Polaron energy as a function of the inverse of the interaction between the impurity and the fermionic bath $k_F a$, with k_F the Fermi momentum of the ideal Fermi gas and a the scattering length between \uparrow and \downarrow atoms. *Solid (black) line*: the variational result solving Eq. 12.5; *dot-dashed (red) line*: first order correction; *dashed (green) line*: second order perturbation theory; diamonds: Fixed-Node Monte-Carlo

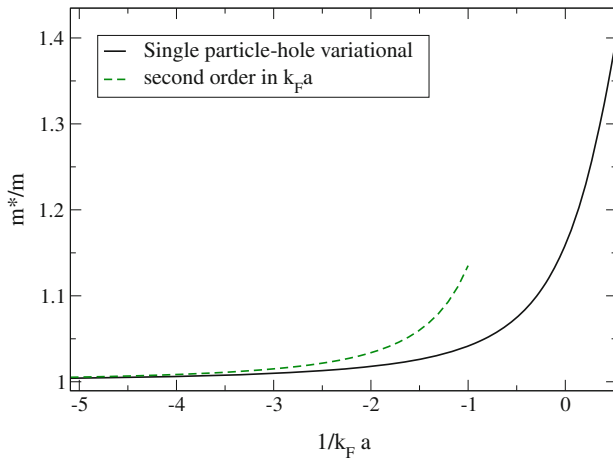


Fig. 12.2 Polaron effective mass m^* as a function of the inverse of the interaction between the impurity and the fermionic bath $k_F a$, with k_F the Fermi momentum of the ideal Fermi gas and a the scattering length between \uparrow and \downarrow atoms. *Solid (black) line*: the variational result solving Eq. 12.5; *dashed (green) line*: second order perturbation theory; diamonds: Fixed-Node Monte-Carlo

smaller, being the effective mass less than 20% bigger than the bare one. In Fig. 12.2 we report the variational and perturbative results (12.2) for the effective mass.

The fact that we can trust the variational calculation is many-fold. Indeed, as can be seen in Fig. 12.1, it agrees very well with the Monte-Carlo calculation, further-

more it has been shown that the inclusion of essentially any number of particle-hole excitation does not significantly change the results [30]. Finally when applied to a one-dimensional system [23, 31] it gives results that are in very good agreement with the exact solution explored by McGuire [32]. It is also worth mentioning that the variational approach is equivalent to a more standard many-body treatment via a T -matrix approximation also known as Brueckner-Hartree-Fock [23, 33].

12.2.2 Non-Homogeneous/Trapped Case

Up to now we have considered the system as being homogeneous. In a real experiment the atoms are trapped by an external electromagnetic field, which in most of the cases can be included in the Hamiltonian by means of a harmonic potential of the form

$$V_{ho}(\mathbf{x}) = \frac{1}{2}m(\omega_x^2 x^2 + \omega_y^2 y^2 + \omega_z^2 z^2). \quad (12.5)$$

The bath can be considered not altered by the presence of the impurity and can be described by an ideal Fermi gas in an harmonic trap. Moreover, most of the times, local density approximation (LDA) [2] is applicable. In such approximation one defines the local chemical potential as $\mu_\uparrow(\mathbf{x}) = (6\pi^2 n_\uparrow)^{2/3} = \mu_\uparrow - V(\mathbf{x})$, where μ_\uparrow is fixed by the number of \uparrow -atoms, i.e., $\mu_\uparrow = (6N_\uparrow)^{1/3} \hbar \bar{\omega}$, with $\bar{\omega}^3 = \omega_x \omega_y \omega_z$ the frequency geometrical average. The impurity is dressed by the bath as described above and can be described by a particle of mass m^* in an effective external potential. Its Hamiltonian is easily written as [34]

$$H_{sp} = \frac{p^2}{2m^*} + V_{ho}(\mathbf{x}) \left(1 + \frac{3}{5}A\right), \quad (12.6)$$

where, for later convenience, we have introduced the dimensionless polaron energy parameter $A = -\mu_\downarrow/(3/5E_F) > 0$, which is $\simeq 1$ at unitarity. The impurity feels a potential stronger than the bare one with the renormalised oscillator frequencies

$$\tilde{\omega}_i = \omega_i \sqrt{\left(1 + \frac{3}{5}A\right) \frac{m}{m^*}}. \quad (12.7)$$

This means, e.g., that the dipole (sloshing) mode of the impurity along, let us say, the x -axis has a larger frequency with respect to the one of the harmonic confinement ω_x , namely

$$\omega_D^{(s)} = \omega_x \sqrt{\left(1 + \frac{3}{5}A\right) \frac{m}{m^*}}. \quad (12.8)$$

For example taking the values obtained by the variational ansatz at unitarity, i.e., $A \simeq 1.01$ and $m^*/m \simeq 1.17$ we have $\omega_D^{(s)}/\omega_x \simeq 1.2$, i.e., an increase of 20% with respect to the bare harmonic oscillator frequency.

It is clear from the above equation that the frequency of the impurity dipole mode (or (*s*)pin-Dipole) provides information about the polaron parameters. First measurements along this line have been reported in [13] and are discussed in Sect. 12.6.

In most of the present chapter we assume that the atoms forming the bath and the impurity atom are just different hyperfine levels of the same atomic specie, thus they are both fermions, have the same mass and they feel the same external potential. It is worth mentioning that the discussion is easily generalised to different atomic species. The value of the polaron parameters A (or μ_\downarrow) and $m_\downarrow^*/m_\downarrow$ depend on the mass ratio m_\downarrow/m_\uparrow [23], which eventually affect the possible configuration in the trap when considering the many-polaron case as we briefly discuss in the Sect. 12.3.3.

12.3 Unbalanced Fermi Gas or Many-Polaron Problem

In this section we discuss what does happen when the concentration of the impurities is finite and the atoms are trapped by an harmonic confinement. We stress that the impurities are also fermions. This fact does not affect clearly the $N+1$ problem, but it makes a huge difference for the kind of phase one has in the finite concentration case. We define the concentration as $x = n_\downarrow/n_\uparrow$ where n_\downarrow and n_\uparrow are the densities of the minority spin- \downarrow atoms and of the majority spin- \uparrow atoms, respectively. We also introduce the polarisation of the system as

$$P = \frac{N_\uparrow - N_\downarrow}{N_\uparrow + N_\downarrow}, \quad (12.9)$$

where N_\uparrow (N_\downarrow) is the number of spin- \uparrow (\downarrow) atoms. Moreover we mainly discuss the case when the gas is at unitarity, i.e., $a \rightarrow \infty$.

12.3.1 Homogeneous Case

The main assumption in describing a system with finite concentration is that even at unitarity the impurities behave as a (almost) non interacting Fermi gas of polarons, or in other words they preserve they fermionic nature and the dressed particles are weakly interacting [16]. Let us start again considering a homogeneous system. The energy functional of the system can be written in the form of the Landau-Pomeranchuk Hamiltonian [16]

$$\begin{aligned} \frac{E(x)}{N_\uparrow} &= \frac{3}{5} E_{F\uparrow} \left(1 - Ax + \frac{m}{m^*} x^{5/3} + Bx^2 \right) \\ &\equiv \frac{3}{5} E_{F\uparrow} \epsilon(x), \end{aligned} \quad (12.10)$$

where N_\uparrow is the number of spin- \uparrow atoms and $E_{F\uparrow} = \hbar^2/2m(6\pi^2 n_\uparrow)^{2/3}$ is the Fermi energy of the spin- \uparrow gas. We repeat again that the first term in Eq. 12.10 corresponds

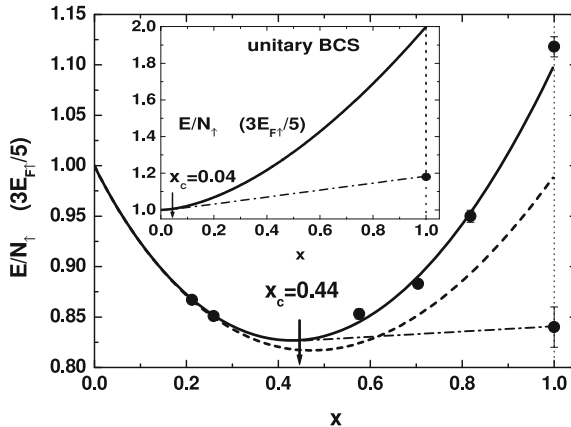


Fig. 12.3 Equation of state of a normal Fermi gas as a function of the concentration x (circles), from [16]. The *solid line* is a best fit to the FN-DMC results, from which the value B of the energy (12.10) is extracted. The *dashed line* corresponds to the non interacting gas of polaron, i.e., Eq. 12.10 with $B = 0$. The *dot-dashed line* is the coexistence line between the normal and the unpolarized superfluid states and the *arrow* indicates the critical concentration x_c above which the system phase separates. For $x = 1$, both the energy of the normal and of the superfluid (diamond) states are shown. In the inset we report the results of a “naive-BCS” theory (see text), in which the superfluid is much more robust

to the energy per particle of the non-interacting gas. The linear term in x gives the single-particle energy of the spin-down particles, while the $x^{5/3}$ term represents the quantum pressure of a Fermi gas of quasi-particles with an effective mass m^* . Eventually, the last term includes the corrections to the free polaron energy. The form of the latter term has been first found by fitting the Monte-Carlo results for finite concentration up to $x = 1$ [16, 29]. The (fitted) energy functional (12.10) is shown in Fig. 12.3, together with the Monte Carlo data and the free polaron energy functional, $B = 0$ (dashed line). The physical interpretation of the x^2 term is still not completely clear, but it can be thought as a quasi-particle forward interaction [35, 36]. It is worth remarking that, while Eq. 12.10 is thought as an expansion of the normal state energy for small concentration, it agrees very well with Monte-Carlo calculations for any values of x [16]. In the present work we use the values $A = 0.99(1)$, $m^* = 1.09(2)$ and $B = 0.14$ calculated in [29], using Fixed-Node Monte-Carlo techniques.

On the other hand we know in the balance case, $x = 1$, and at $T = 0$, the system is superfluid. The equation of state of a homogeneous unpolarized superfluid at unitarity is simply given by the energy of an ideal Fermi gas multiplied by an universal parameter (see, e.g., [2, 3])

$$\frac{E_S}{N_S} = \xi_S \frac{3}{5} \frac{\hbar^2}{2m} (6\pi^2 n_S)^{2/3} \equiv \epsilon_S(n_S), \quad (12.11)$$

where N_S is the number of atoms in the superfluid phase and the universal parameter ξ_S has been calculated by different techniques, e.g., employing Quantum Monte Carlo simulations [37, 38] or diagrammatic techniques [39]. It has been also measured experimentally. We rely in what follows on the Monte Carlo value $\xi_S \simeq 0.42$. It means that if we assume that the system admits only these two phases, namely the unpolarized superfluid and the partially polarized normal phase, there exists a critical value of the concentration, x_c , at which the superfluid starts to be nucleated in the normale state. The transition between the normal and the superfluid phase is of first order nature and the equilibrium of the two phases is found by imposing chemical and mechanical equilibrium. At constant volume V a further increase of the number of the minority atoms turns in a increase of the superfluid part. The equilibrium pressure reads

$$\frac{\partial E(x)}{\partial V} = \frac{\partial E_S}{\partial V} \quad (12.12)$$

and using Eqs. 12.11 and 12.10, it provides the relation between the superfluid density and the majority atom density in the normal phase

$$\frac{n_S}{n_\uparrow} = \left(\frac{\epsilon(x)}{2\xi_S} \right)^{3/5}. \quad (12.13)$$

The chemical potential equilibrium is equivalent to state that the chemical potential of the superfluid is equal to the sum of the chemical potential of the majority, μ_\uparrow , and of the minority, μ_\downarrow , atoms. From Eq. 12.11 one has $\xi_S \hbar^2 / (2m) (6\pi^2 n_S)^{2/3} = \mu_\uparrow + \mu_\downarrow$. Eventually one finds that the critical concentration is given by the solution of the equation

$$\frac{3}{5} (x_c - 1) \epsilon'(x_c) = \epsilon(x_c) - 2\xi_S \left(\frac{\epsilon(x_c)}{2\xi_S} \right)^{2/5}, \quad (12.14)$$

where the prime means the derivative with respect to the concentration x . In this way we determine the critical concentration to be $x_c \simeq 0.44$ and interestingly enough the density jump between the superfluid and the majority component is almost not existent being $n_S/n_\uparrow \simeq 1.02$. This is peculiar of the equal mass case, while for different masses the jump can be pretty large (see Sect. 12.3.3). The coexistence line, shown also in Fig. 12.3 by the dashed-dot line, is obtained by minimizing the energy at a constant volume of a superfluid coexisting with a normal phase with concentration x_c . To show the importance of properly including the interaction in the normal phase, in the inset of Fig. 12.3 we report the same results but using the most “naive-BCS” theory. Namely we take the BCS result for the superfluid energy at unitarity (i.e., without any Hartree term) and the normal phase is just a two-component unbalance free Fermi gas. The normal phase would be practically never realised.

Before moving to the trapped case, a couple of remarks on the unstable strongly interacting normal phase at $x = 1$. are due. Such a phase has an energy which, being at unitarity, can be written as the one for the superfluid

$$\frac{E_n}{N} = \xi_n \frac{3}{5} \frac{\hbar^2}{2m} (6\pi^2 n)^{2/3} \equiv \epsilon_n(n), \quad (12.15)$$

with a different universal interaction parameter ξ_n that was also calculated via Monte-Carlo technique in [37, 38]. Such a phase is difficult to get in the lab, although it was suggested that it could emerge as an equilibrium phase in a rotating trap [40–42]. However, such a phase is not just of academic interest. Indeed it turns out that it is possible to probe such a phase experimentally, being connected to the $T \neq 0$, $P = 0$ and to the $T = 0$, $P \neq 0$ normal phase of the gas. This has been shown by the very recent analysis of some extrapolated quantities measured by the ENS group (C. Salomon, private communication).

12.3.2 Non-Homogeneous/Trapped Case

In a trap the local chemical potential fixes the sequence of phases present as a function of the distance from the trap centre. A good way to understand this feature is to convert the density relations to the chemical potential ones, i.e., to draw the grand canonical phase diagram in terms of total chemical potential $\mu = (\mu_\uparrow + \mu_\downarrow)/2$ and effective magnetic field $h = (\mu_\uparrow - \mu_\downarrow)/2$ as sketched in Fig. 12.4. In this respect the superfluid to normal phase transition is characterise by $(h/\mu)_c = 0.96$ (continuous red line in Fig. 12.4) or $\eta_c = (\mu_\downarrow/\mu_\uparrow)_c = 0.02$. The earlier value is precisely the Chandrasekhar–Clogston limit for our unitary Fermi gas. We also draw the line of the transition between the normal mixed phase and the fully polarised one which corresponds to the chemical potential ratio for a single impurity $h/\mu = (1 - 3/5A)/(1 + 3/5A) = 3.94$ (dashed green line in Fig. 12.4). We call $\mu_{\uparrow,\downarrow}^0$ the chemical potentials in the centre of the trap. The chemical potential $\mu = (\mu_\uparrow^0 + \mu_\downarrow^0)/2 - V(\mathbf{x})$ decreases going outward in the trap, while $h = (\mu_\uparrow^0 - \mu_\downarrow^0)/2$ is constant, and thus in a trap we explore the phase diagram along a straight line parallel to μ . In other words we can explore the whole phase diagram in a single shot and this represents a very stringent test for any theory. It is clear that it could be that some of these phases occupy a very narrow space region that are not detectable in actual experiments.

We see from Fig. 12.4 that if h is not too large we expect to have a superfluid in the centre of the trap surrounded by a shell of normal phase with decreasing concentration x going outward in the trap. When h is large enough no superfluid is present. This $T = 0$ behaviour is in agreement with what has been found experimentally [8–10, 13, 15, 43].

A quantitative comparison with experiments can be done by calculating the density profiles, which in a trap are given by the following LDA expression

$$\frac{\mu_\uparrow^0 + \mu_\downarrow^0}{2} = \xi_S \frac{\hbar^2}{2m} (6\pi^2 n_S)^{2/3} + V(\mathbf{r}) \quad (12.16)$$

in the superfluid region and by

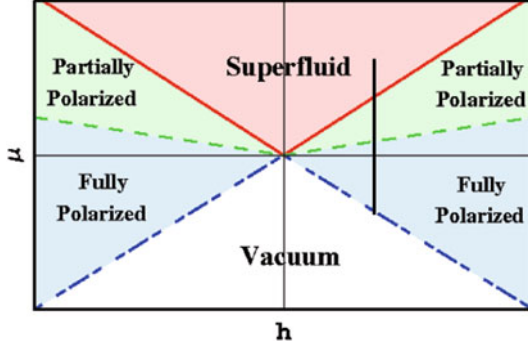


Fig. 12.4 The $\mu-h$ phase diagram. The first order phase transition is indicated by a *continuous line* and where we report also the second order transition between the mixed normal phase and the fully polarised gas. The straight *black line* are the phases present in the trapped gas. The total chemical potential μ decreases moving outward in the trap, while h is constant and fixed by the polarization P . If P is not too large one has a superfluid in the center of the trap, then a normal mixed phase and eventually a fully polarised Fermi gas of the majority atoms

$$\mu_{\uparrow}^0 = \left(\epsilon(x) - \frac{3}{5}x\epsilon'(x) \right) \frac{\hbar^2}{2m} (6\pi^2 n_{\uparrow})^{2/3} + V(\mathbf{r}), \quad (12.17)$$

$$\mu_{\downarrow}^0 = \frac{3}{5}\epsilon'(x) \frac{\hbar^2}{2m} (6\pi^2 n_{\uparrow})^{2/3} + V(\mathbf{r}), \quad (12.18)$$

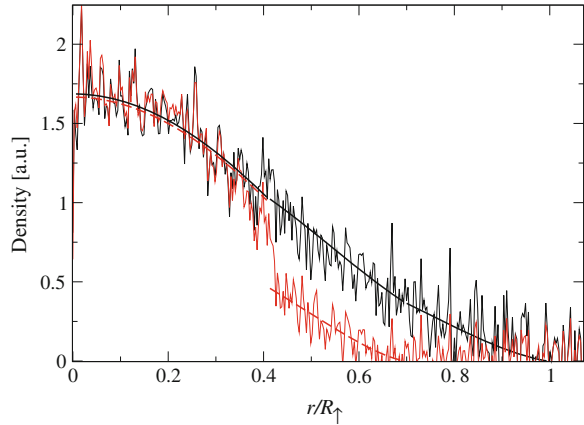
in the region occupied by the normal phase. The value of μ_{\uparrow}^0 and μ_{\downarrow}^0 are determined, as usual, by fixing the number of atoms N_{\uparrow} and N_{\downarrow} . The border between the superfluid and the normal phase region is given by the locus of points \mathcal{R} satisfying

$$\frac{\mu_{\downarrow}^0 - V(\mathcal{R})}{\mu_{\uparrow}^0 - V(\mathcal{R})} = \eta_c. \quad (12.19)$$

In a spherical trap ($\omega_x = \omega_y = \omega_z = \omega_0$) we can identify \mathcal{R} with the radius of the superfluid, R_S . The first result one can get is the critical polarization above which the superfluid disappears from the trap. It happens when the density ratio in the centre of the trap is equal to the critical value x_c . It turns out that $P_c = 0.77$ and this prediction is in very good agreement with experiments. An even stronger test for the theory is the direct comparison of the density profiles, which can be obtained experimentally via the so called Abel transform [44]. In Fig. 12.5 we show the comparison between theory and experiment. The agreement is extremely good and the jump in going from the equal density superfluid to the mixed normal phase is evident and in agreement with the CC limit $x_c \simeq 0.44$.

A deeper insight in the density profiles and a link with the single polaron problem can be obtained by solving Eqs. 12.17 and 12.18 in the high polarisation case, i.e., $N_{\uparrow} \gg N_{\downarrow}$. To the leading order in x , we get

Fig. 12.5 Density profiles for a polarization $P = 44\%$. Theory: *solid black line* (*dashed red line*) is the spin- \uparrow (spin- \downarrow) density. Experiment: the *black (red)* line is the spin- \uparrow (spin- \downarrow) density as reported in [10]. The density jump in the \downarrow component is clearly visible



$$\mu_{\uparrow}^0 = \frac{\hbar^2}{2m} (6\pi^2 n_{\uparrow})^{2/3} + V(\mathbf{r}), \quad (12.20)$$

$$\mu_{\downarrow}^0 + \frac{3}{5} A \mu_{\uparrow}^0 = \frac{\hbar^2}{2m^*} (6\pi^2 n_{\downarrow})^{2/3} + V(\mathbf{r}) \left(1 + \frac{3}{5} A \right), \quad (12.21)$$

yielding the non-interacting value $\mu_{\uparrow}^0 = (6N_{\uparrow})^{1/3} \hbar \omega_0$ for the chemical potential of the majority component. The above equations show that both the majority and the minority components have an ideal Fermi gas profile, the latter being described by a renormalised mass m^* and feeling a renormalised external potential. The radius of the minority component is hence quenched by the interaction to the value

$$R_{\downarrow} = R_{\downarrow}^0 \left[\frac{m^*}{m} \left(1 + \frac{3}{5} A \right) \right]^{-1/4}, \quad (12.22)$$

where $R_{\downarrow}^0 = (48N_{\downarrow})^{1/6} \sqrt{\hbar/(m\omega_0)}$ is the Thomas-Fermi radius of the ideal Fermi gas. These results are easily understood in terms of the effective single quasi-particle Hamiltonian (12.6).

12.3.3 Different Mass Case: Fermi Mixture

The analysis developed in the previous sections can be extended to Fermi mixtures, where the two spin species correspond to different atoms, as, e.g., ${}^6\text{Li} - {}^{40}\text{K}$ [45, 46]. We will focus mainly on the unitarity regime. Since we are interested in describing the normal phase of the system, we assume again that the only two possible phases are an unpolarised superfluid and a mixed normal phase [47], whose description is

based on the polaron concept. The calculation of the polaron parameters is the same as the one explained in Sect. 12.2 just with the impurity mass m_\downarrow different from the mass m_\uparrow of the atoms forming the bath. In this case we have a new parameter given by the mass ratio $r = m_\downarrow/m_\uparrow$.

Let us here make two remarks on the polaron energy. First of all there exists an approximate easy expression for the binding energy as a function of $k_F a$ and r , which is obtained in the limit for large ratio $\rho = |\mu_\downarrow|/\mu_\uparrow$ [23]

$$\frac{1}{k_F a} = \sqrt{\frac{\rho r}{1+r}} - \frac{2}{3\pi} \frac{1+r}{\rho r}, \quad (12.23)$$

Although it has been obtained in the large ρ limit, the above expression (i) recovers the weakly interacting result (12.2) (with the proper reduced mass), (ii) is in pretty good agreement with the known value at unitarity where it reads $\rho = (1+1/r)(2/3\pi)^{2/3}$ and (iii) recovers the correct two-body binding energy $\rho = (1+1/r)(1/k_F a)^2$ for small positive- a . Second, the infinite mass ratio case admits an exact solution. Indeed, since the impurity is static in this case we can use the Fumi's theorem [48] which relates the impurity energy to an integral over the phase shifts δ_l of the scattering states of the atoms in the bath:

$$\mu_\downarrow = -\frac{\hbar^2}{m\pi} \int_0^{k_F} k \sum_l \delta_l(k) dk. \quad (12.24)$$

For low energy atoms only s -wave phase shifts are relevant and $\tan(\delta_0(k)) = -ka$. From (12.24) we get

$$\rho = \frac{1}{\pi} \left(\frac{1}{k_F a} - \left(1 + \frac{1}{(k_F a)^2} \right) \arctan(k_F a) \right). \quad (12.25)$$

In Figs. 12.6 and 12.7 the absolute value of the polaron energy and effective mass, respectively, are shown for different values of r . The main message is that the lighter is the impurity, the larger the effect of the bath on it. This behaviour is shown at unitarity in the insets, where for the polaron energy we show also the approximate result obtained from Eq. 12.23 for $k_F a \rightarrow \infty$.

Once the polaron parameters are known one can write a Landau-Pomeranchuk energy as for the equal mass case

$$\begin{aligned} \frac{E(x, \kappa)}{N_\uparrow} &= \frac{3}{5} E_{F\uparrow} \left(1 - A(\kappa)x + \frac{F(\kappa)^{-1}}{\kappa} x^{5/3} + B(\kappa)x^2 \right) \\ &= \frac{3}{5} E_{F\uparrow} g(x, \kappa) \equiv \epsilon_n(x, \kappa), \end{aligned} \quad (12.26)$$

where the term in x^2 has been added in analogy with the equal mass case, and its coefficient determined by imposing that at $x = 1$ Eq. 12.26 reduces to the energy of the normal (balanced) state Eq. 12.15. Indeed for both the unpolarised superfluid

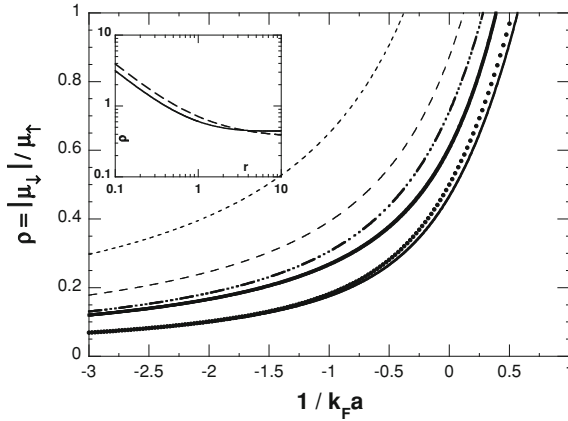
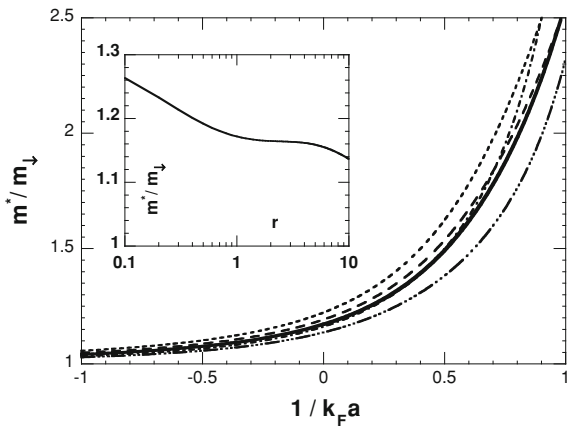


Fig. 12.6 Polaron energy as a function of $1/k_F a$ for various mass ratios r . *Black curves from top to bottom: polaron energy for mass ratio $r = 0.25, 0.5, 1$ (solid thick line), and ∞ (lower solid line). The dashed-triple dotted blue line above the equal mass line is the interpolating approximation Eq. 12.23. The dotted red line just above the infinity mass impurity line is the exact result Eq. 12.25. The inset compares, at unitarity, the approximation Eq. 12.23 (dashed line) with the numerical results (solid line) as a function of the mass ratio r*

Fig. 12.7 Relative effective mass m^*/m_\downarrow as a function of $1/k_F a$ for various mass ratios r . Same conventions as in Fig. 12.6 for $r = 0.25, 0.5,$ and 1 . The dashed-dotted line is $r = 4$, and the dashed-triple-dotted line is $r = 10$. The inset shows the effective mass as a function of r at unitarity



phase at unitarity and the normal $x = 1$ phase the universal parameter $\xi_{S,n}$ depends very weakly on the mass ratio once the free Fermi gas energy is expressed in terms of the reduced mass.

Following the procedure explained in Sect. 12.3 one finds the critical concentration at which the system starts nucleating a superfluid. The results are reported in Fig. 12.8. For comparison we also report the result obtained by the naive-BCS mean-field calculation, as discussed in the previous section, where the interaction in the normal phase is not taken into account and the BCS value $\xi_{S(BCS)} = 0.59$ for the superfluid phase is consistently used. Interesting enough, within the present

Fig. 12.8 Critical concentration $x_c(\kappa)$ for a homogeneous system as a function of the mass ratio κ : *upper line* is obtained using the equation of state (12.26), while the *lower dashed line* is derived from the BCS mean-field solutions at unitarity (see text)

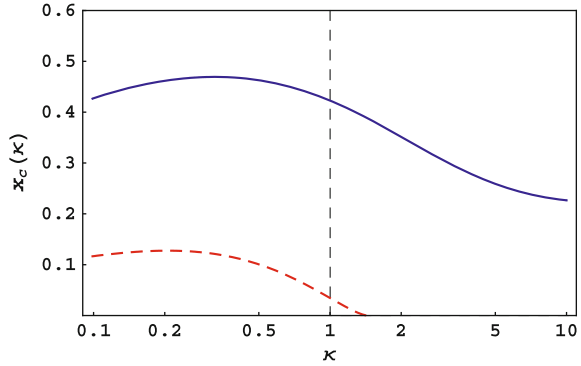
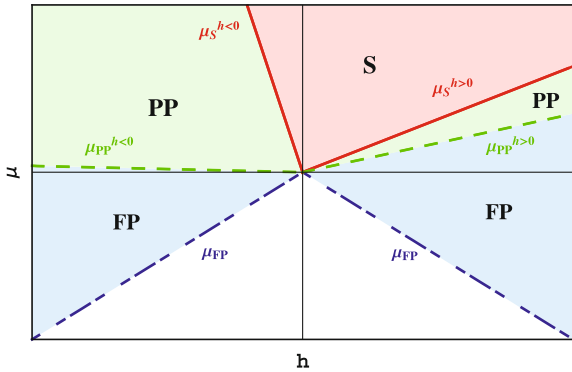


Fig. 12.9 (Color online) For $\kappa = 2.2$ the phase diagram is asymmetric. Shown are the superfluid S (solid red lines), partially polarized PP (dashed green) and fully polarized FP (dot-dashed blue) regions



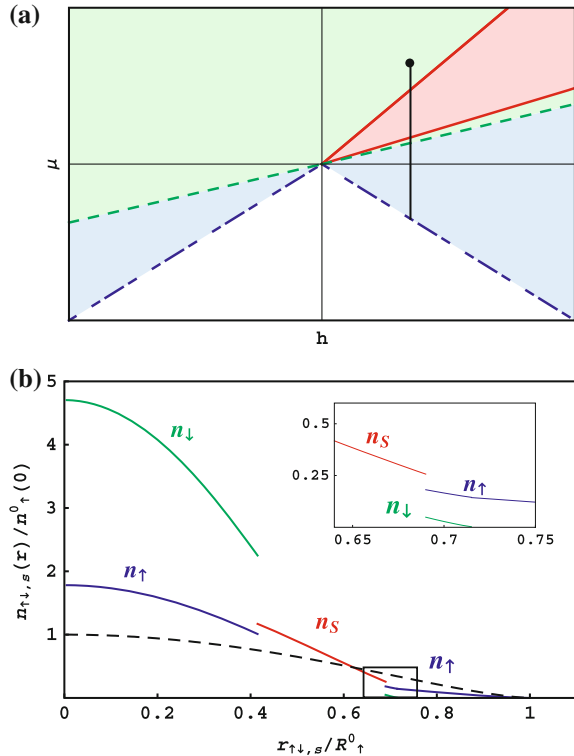
approach—and also within BCS mean-field theory—the critical concentration has a non-monotonic behaviour. The range of values is also pretty limited. It is more interesting the behaviour of the density change between the superfluid and the normal phase. For the equal mass case is given by Eq. 12.13 and it is very close to unity. For the unequal mass case Eq. 12.13 reads

$$\frac{n_{\uparrow}(x, \kappa)}{n_S(\kappa)} = \left(\frac{(1 + \frac{1}{\kappa})\xi_S}{g(x, \kappa)} \right)^{3/5}. \tag{12.27}$$

For instance for a mixture ${}^6\text{Li} - {}^{40}\text{K}$ with more Lithium present, i.e., $\kappa \simeq 6.67$, one has $x_c(6.67) = 0.24$ and a density jump $n_{\text{Li}}/n_S = 0.71$.

The grand-canonical phase diagram is in this case asymmetric with respect to the change $h \rightarrow -h$ and for $\kappa = 2.2$ is shown in Fig. 12.9. This feature together with the possibility to have different confinement potentials for the two atomic species, i.e., different trapping frequencies for a harmonic confinement $\omega_{i,\uparrow} \neq \omega_{i,\downarrow}$, $i = x, y, z$, allows for more available configurations for trapped gases, with respect to the homonuclear case described before [47]. Even for equal trapping potentials interesting configurations can appear. As an example here we consider the case of a ${}^6\text{Li} - {}^{40}\text{K}$

Fig. 12.10 (Color online) **a** Phase diagram for $\kappa = 6.7$, corresponding to a $^{40}\text{K} - ^6\text{Li}$ mixture. **b** Density profiles in units of the central density of the noninteracting \uparrow -gas (*dashed line*) for $P = -0.13$. The inset shows a zoom of the outer superfluid-“light” normal border



mixture. Generally if $\mu_{\downarrow}/\mu_{\uparrow} > 1/\eta_c(1/\kappa)$ the trapped system will consist of a three-shell configuration, where the superfluid is sandwiched between a “heavy” normal phase (heavy spin- \downarrow are the majority) at the center of the trap, and a “light” normal phase (light spin- \uparrow are the minority) in the outer trap region [47, 49–51].

The phase diagram and the relative density profiles of the system are shown in Fig. 12.10, for a polarization $P = -0.13$. The density jump between the superfluid and both normal phases previously discussed are clearly visible.

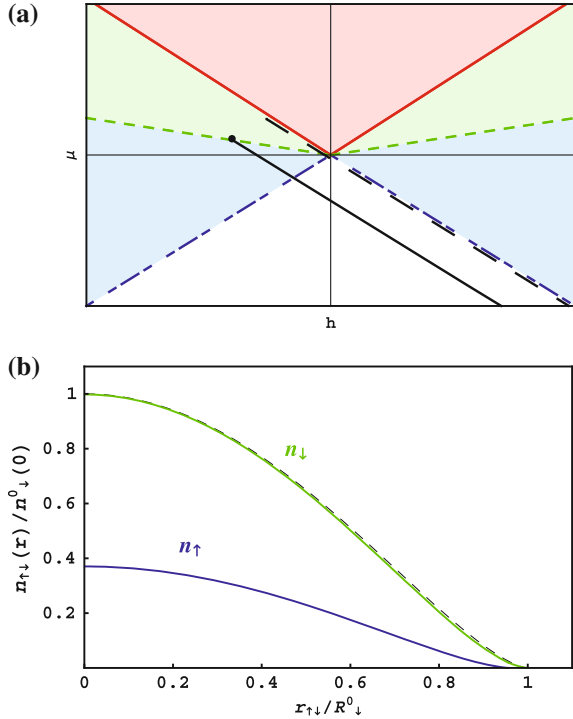
Another interesting case, in view of studying the normal phase of a strongly interacting Fermi mixture, is when one of the component is not trapped, but just confined due to interatomic forces as shown in Fig. 12.11.

In order to get a better insight into such configuration we can again refer to the highly unbalanced case $N_{\downarrow} \gg N_{\uparrow}$ (black solid line in Fig. 12.11a). The densities are easily found to be

$$\mu_{\downarrow}^0 = \frac{\hbar^2}{2m} (6\pi^2 n_{\downarrow}(\mathbf{r}))^{2/3} + V_{\downarrow}(\mathbf{r}), \quad (12.28)$$

$$\mu_{\uparrow}^{0'} = \frac{\hbar^2}{2m^*} (6\pi^2 n_{\uparrow}(\mathbf{r}))^{2/3} + V_{\uparrow}'(\mathbf{r}), \quad (12.29)$$

Fig. 12.11 (Color online) No trapping for the spin- \uparrow component, i.e., $\omega_{\uparrow, i} = 0$ and $\kappa = 1$. **a** Phase diagram. **b** Density profiles in units of the central density of the noninteracting gas for a polarization $P = -0.5$



where $\mu_{\uparrow}^{0r} = \mu_{\uparrow}^0 + \frac{3}{5}A\mu_{\downarrow}^0$, $V_{\uparrow}'(\mathbf{r}) = V_{\uparrow}(\mathbf{r}) + \frac{3}{5}AV_{\downarrow}(\mathbf{r})$ and $A \equiv A(\kappa = 1)$. From these equations it is clear that if $V_{\uparrow} \rightarrow 0$, the \uparrow -atoms feel nevertheless the renormalized potential $\frac{3}{5}AV_{\downarrow}(\mathbf{r})$ and are confined due to the interaction with the \downarrow -component.

12.4 RF Spectroscopy

An invaluable tool to prepare, manipulate and probe ultracold gases is the RF spectroscopy. There have been quite a number of experimental and theoretical papers discussing it to which the reader is refer to for all the details and subtleties (see [52] and references therein). In the following we present a short digression on RF spectroscopy as a tool to probe polaron properties.

Let us consider as usual in this review that the bath and the impurity are labelled by $|\uparrow\rangle$ and $|\downarrow\rangle$, respectively, and that the RF field couples the latter with a third state $|3\rangle$ which does not interact with the bath. Since the RF field has a very long wavelength (zero momentum transferred) and is constant over the size of the atomic cloud the RF operator reads

$$\hat{O} = \hbar\Omega_R \int d^3\mathbf{x} \hat{\psi}_3^\dagger(\mathbf{x})\hat{\psi}_\downarrow(\mathbf{x}) + h.c., \quad (12.30)$$

where Ω_R is the Rabi frequency and $\hat{\psi}_3(\mathbf{x})$ and $\hat{\psi}_\downarrow(\mathbf{x})$ are the field operators for the atoms in the internal state $|3\rangle$ and $|\downarrow\rangle$, respectively. According to Fermi's golden rule the RF spectrum $\Gamma(\omega)$ for the system prepared in the state $|\Phi\rangle$ is

$$\Gamma(\omega) = \frac{2\pi}{\hbar} \sum_f |\langle f|\hat{O}|\Phi\rangle|^2 \delta(\hbar\omega - E_f + E_i), \quad (12.31)$$

where the sum is over all the possible final states $|f\rangle$ and ω is measured with respect to the bare frequency $\omega_{\downarrow 3}$ of the $|\downarrow\rangle \rightarrow |3\rangle$ atomic transition. The spectrum is easily calculated assuming a single impurity and the variational state Eq. 12.3. We are left with two contribution for the spectrum [17]

$$\Gamma(\omega) = 2\pi \hbar\Omega_R^2 \left[|\phi_0^p|^2 \delta\left(\hbar\omega + \epsilon_\downarrow + \frac{p^2}{2m^*} - \frac{p^2}{2m}\right) \right. \quad (12.32)$$

$$\left. + \sum_{\substack{k > k_F \\ q < k_F}} |\phi_{\mathbf{q}k}^p|^2 \delta\left(\hbar\omega + \epsilon_\downarrow + \frac{p^2}{2m^*} - \epsilon_{\uparrow k} + \epsilon_{\uparrow q} - \epsilon_{\downarrow \mathbf{p}+q-k}\right) \right], \quad (12.33)$$

where ϵ_\downarrow is the single polaron energy. The first contribution is a delta-peak at $\epsilon_\downarrow - (1 - m/m^*)p^2/2m$ [34], i.e., at the polaron rest energy plus the contribution due to the fact that the effective mass is different from the bare one, and with a weight given by the quasi-particle residue $|\phi_0^p|^2 = Z_p$. Since $\epsilon_\downarrow < 0$ the RF field has to supply additional energy for the transition to occur with respect to the bare one $\hbar\omega_{\downarrow 3}$. The second term instead consists of a continuum of frequencies. Such a structure is typical in Landau theory of Fermi liquids. Indeed for free particles one has only the first term, since the spectral function is simply a delta function. For an interacting Fermi system the spectral function of a quasi-particle in the limit of infinite life-time can be written as a coherent delta-function term plus an incoherent part. In actual experiments one has always a finite concentration of the minority component and, due to the effective mass this leads to a broadening of the delta peak. Indeed, as we have seen in the previous sections, the system can be described as a free Fermi gas of polarons. The spectrum is then just the sum of the single polaron spectrum (12.33). The coherent part reads [17]

$$\Gamma^{\text{coh}}(\omega) = 2\pi \hbar\Omega_R^2 \sum_{p < k_{F\downarrow}} |\phi_0^p|^2 \delta\left(\hbar\omega + \mu_\downarrow + \frac{p^2}{2m^*} - \frac{p^2}{2m}\right). \quad (12.34)$$

where $p_{F\downarrow}$ is the Fermi momentum of the minority component. Thus the spectrum starts at ϵ_\downarrow and goes again to zero at $\hbar\omega = -\epsilon_\downarrow + (1 - m/m^*)p_{F\downarrow}^2/2m$. A more detailed and refined description of the behaviour of RF-spectrum at finite concentration

can be found in, e.g., [53, 54]. The RF-spectrum measurement has been indeed carried out and in this way was possible to obtain the first observation of Fermi polaron physics with the measurement of its energy, effective mass and quasi-particle residue [17].

12.5 Collisional Properties of the Normal Phase

In the previous sections we introduced the polaron concept as an infinite life-time quasi-particle. In the same spirit we have briefly discussed the *out of phase* oscillations of the impurity with respect to the ideal Fermi gas (that are extensively discussed in Sect. 12.6) and we extended the analysis to finite concentration. We considered the system as being perfectly collisionless, by assuming that the only effect of the bath is to renormalise the potential and the mass of the impurity. Generally this is not the case and when the impurity moves with a relative speed in the bath we have a damping of the counterflow determined by the rate at which momentum is transferred between the two components. Such a rate is related to the quasi-particle scattering amplitude which, in the weakly interacting regime, is proportional to the scattering length a . In the strongly interacting case one expects that the system is more easily in a collisional (hydrodynamic) regime. At finite temperature even the polaron at rest has a finite life-time since real collisions can take place. A finite life-time changes the delta-peak in the coherent part of the spectral function to just a function peaked around the polaron energy and, thus, it could be extracted from RF measurements as described in the previous Section.

In this section we use the concepts of Fermi liquid theory to describe the scattering amplitude and the momentum relaxation time (see e.g., [55]). The elementary excitations of our system are quasi-particles with effective mass m_{\downarrow}^* . We take the minority component to have a mean velocity \mathbf{v} with respect to the majority component corresponding to a total momentum per unit volume $\mathbf{P}_{\downarrow} = n_{\downarrow} m_{\downarrow}^* \mathbf{v}$.

We define the momentum relaxation time τ_P by the relation

$$\frac{d\mathbf{P}_{\downarrow}}{dt} = -\frac{\mathbf{P}_{\downarrow}}{\tau_P}. \quad (12.35)$$

and calculate τ_P by assuming that both components are in thermal equilibrium. Introducing the single particle energies $\epsilon_{\mathbf{p}'\uparrow} = p'^2/2m_{\uparrow}$ and $\epsilon_{\mathbf{p}\downarrow} = p^2/2m_{\downarrow}^*$ the thermal equilibrium is described by the distribution functions $n_{\mathbf{p}'\uparrow} = f[\beta(\epsilon_{\mathbf{p}'\uparrow} - \mu_{\uparrow})]$ and $n_{\mathbf{p}\downarrow} = f[\beta(\epsilon_{\mathbf{p}\downarrow} - \mathbf{p} \cdot \mathbf{v} - \mu_{\downarrow})]$ with $\beta = 1/k_B T$ and where $f(x) = 1/(e^x + 1)$ is the Fermi distribution function. The term $\mathbf{p} \cdot \mathbf{v}$ boosts the \downarrow -atom distribution function by a velocity \mathbf{v} . The momentum of the impurities changes due to collisions with the majority atoms according to

$$\mathbf{p}_{\downarrow} + \mathbf{p}'_{\uparrow} \longrightarrow (\mathbf{p} - \mathbf{q})_{\downarrow} + (\mathbf{p}' + \mathbf{q})_{\uparrow} \quad (12.36)$$

If we call U the momentum independent scattering amplitude for such a process the rate of change of the minority momentum may be written as

$$\begin{aligned} \frac{d\mathbf{P} \downarrow}{dt} = & -\frac{2\pi|U|^2}{V^3} \sum_{\mathbf{p}, \mathbf{p}', \mathbf{q}} \mathbf{p} [n_{\mathbf{p}\downarrow} n_{\mathbf{p}'\uparrow} (1 - n_{\mathbf{p}-\mathbf{q}\downarrow}) (1 - n_{\mathbf{p}'+\mathbf{q}\uparrow}) \\ & - n_{\mathbf{p}-\mathbf{q}\downarrow} n_{\mathbf{p}'+\mathbf{q}\uparrow} (1 - n_{\mathbf{p}\downarrow}) (1 - n_{\mathbf{p}'\uparrow})] \delta(\epsilon_{\mathbf{p}\downarrow} + \epsilon_{\mathbf{p}'\uparrow} - \epsilon_{\mathbf{p}-\mathbf{q}\downarrow} - \epsilon_{\mathbf{p}'+\mathbf{q}\uparrow}), \end{aligned} \tag{12.37}$$

where V is the volume of the system. The second term on the right hand side of (12.37) correspond to the inverse of the process (12.36).

The effective interaction U may be estimated from thermodynamic arguments. Since the momenta of the \downarrow -atoms are assumed to be much less than the Fermi momentum of the \uparrow -atoms, the quasiparticle interaction may be taken to be independent of the angle between the quasiparticle momenta. To estimate the scattering amplitudes in terms of Landau parameters it is generally necessary to allow for additional processes due to screening by particle-hole pairs [56]. However, since we assume that $n_{\downarrow} \ll n_{\uparrow}$, these processes may be neglected, and we take the scattering amplitude to be independent of the direction of the momenta of the quasiparticles and equal to the Landau quasiparticle interaction averaged over the angle between the momenta of the two quasiparticles, i.e., $U = f_{\uparrow\downarrow}^0$ in the standard notation of Landau Fermi liquid theory. The latter may be determined from the energy as a function of the densities of the two components:

$$U = f_{\uparrow\downarrow}^0 = \frac{\partial^2 E(x)/V}{\partial n_{\uparrow} \partial n_{\downarrow}} = \frac{\partial \mu_{\downarrow}}{\partial n_{\uparrow}} \longrightarrow U = \frac{2\pi^2}{m_{\uparrow} k_{F\uparrow}} \gamma, \tag{12.38}$$

where $E(x)$ is the energy (12.10) of the polarised system, $k_{F\sigma} = (6\pi^2 n_{\sigma})^{1/3}$ and we define

$$\gamma = -\frac{3}{5} A \left(1 + \frac{3n_{\uparrow}}{2A} \frac{\partial A}{\partial n_{\uparrow}} \right). \tag{12.39}$$

For the case of a resonant interaction, $\gamma = -3/5 A$ and $U = -(6\pi^2 A/5)/(m_{\uparrow} k_{F\uparrow})$. This is very different from the effective interaction at low densities (weak interacting case), which is proportional to a . The previous result tell us already that there exists a range of temperature for which the unitary polarised Fermi gas is collisionless.

It is convenient to rewrite the expression (12.37) in terms of response function. By introducing the quantity $\omega_{\mathbf{q}} = \mathbf{q} \cdot \mathbf{v}$, using the relation $n_{\mathbf{p}}(1 - n_{\mathbf{p}-\mathbf{q}}) = (n_{\mathbf{p}} - n_{\mathbf{p}-\mathbf{q}}) / \{1 - \exp[\beta(\epsilon_{\mathbf{p}} - \epsilon_{\mathbf{p}-\mathbf{q}})]\}$, and taking the continuum limit we obtain

$$\frac{d\mathbf{P} \downarrow}{dt} = -|U|^2 \int \frac{d^3 \mathbf{q} \mathbf{q}}{(2\pi)^2} \int_{-\infty}^{\infty} d\omega \frac{\text{Im} \chi_{\downarrow}(q, \omega_{\mathbf{q}} \omega) \text{Im} \chi_{\uparrow}(q, \omega)}{(1 - e^{\beta(\omega - \omega_{\mathbf{q}})})(1 - e^{-\beta\omega})}, \tag{12.40}$$

where

$$\text{Im} \chi_{\sigma}(q, \omega) = \int \frac{d^3 p}{(2\pi)^3} (n_{\mathbf{p}\sigma} - n_{\mathbf{p}+\mathbf{q}\sigma}) \delta(\omega + \epsilon_{\mathbf{m}\sigma} - \epsilon_{\mathbf{p}+\mathbf{q}\sigma}) \tag{12.41}$$

is, apart from a factor of π , the imaginary part of the Lindhard function, and the distribution functions are now global equilibrium ones without the boost for the down-atoms.

12.5.1 $T = 0$

Let us start by considering the zero-temperature momentum relaxation rate. Due to the Bose factors in (12.40) one has the condition $0 \leq \omega \leq \omega_{\mathbf{q}}$. Depending on the ratio between the momentum of the minority cloud and its Fermi momentum, i.e., $m_{\downarrow}^* v / k_{F\downarrow}$, it is possible to distinguish two important limiting regimes for which simple expressions for τ_P can be obtained.

12.5.1.1 Low Velocity Regime, $m_{\downarrow}^* v \ll k_{F\downarrow}$

In this case the significant contribution to (12.40) comes from $q \leq 2k_{F\downarrow}$ with a small energy transfer $\omega_{\mathbf{q}} \ll k_{F\downarrow}^2 / 2m_{\downarrow}^*$. We can then use $\text{Im}\chi_{\sigma}(q, \omega) = m_{\sigma}^{*2} \omega / (4\pi^2 q)$ and the resulting integrals in (12.40) yield

$$\frac{1}{\tau_P} = \frac{4\pi}{25} |\gamma|^2 \left(\frac{k_{F\downarrow}}{k_{F\uparrow}} \right)^2 m_{\downarrow}^* v^2 = \frac{4\pi}{25} \frac{1}{\tau_0} \left(\frac{m_{\downarrow}^* v}{k_{F\downarrow}} \right)^2, \quad (12.42)$$

where $1/\tau_0 = |\gamma|^2 k_{F\downarrow}^4 / m_{\downarrow}^* k_{F\uparrow}^2$.

12.5.1.2 High Velocity Regime, $k_{F\downarrow} \ll m_{\downarrow}^* v \ll k_{F\uparrow}$

In this case we can again carry out the integrations in (12.40) and obtain

$$\frac{1}{\tau_P} = \frac{2\pi}{35} |\gamma|^2 \frac{m_{\downarrow}^{*3} v^4}{k_{F\uparrow}^2} = \frac{2\pi}{35} \frac{1}{\tau_0} \left(\frac{m_{\downarrow}^* v}{k_{F\downarrow}} \right)^4. \quad (12.43)$$

More generally, the scaled relaxation time $\tilde{\tau}_P \equiv \tau_P / \tau_0$ depends only on the variable $\tilde{v} = m_{\downarrow}^* v / k_{F\downarrow}$ provided $m_{\downarrow}^* v \ll k_{F\uparrow}$ and its dependence, aside from the prefactors, is the same as the one obtained for a (balanced) neutral Fermi liquid (see, e.g., [55]).

12.5.2 $T \neq 0$

We now turn to non-zero temperature. Although current experiments on polarised gases achieve very low temperatures in the highly polarised case it can happen that

the actual temperature is much smaller than the larger Fermi temperature, related to the majority component, but still of the same order or larger than the smaller one, related to the polaron gas. In the following we analyse only the case when both components are degenerate, i.e., $T \ll T_{F\downarrow} \ll T_{F\uparrow}$ with $k_B T_{F\downarrow} = k_{F\downarrow}^2/2m_{\downarrow}^*$ and $k_B T_{F\uparrow} = k_{F\uparrow}^2/2m_{\uparrow}$. For a discussion on the high-temperature and intermediate regimes the reader can consult Ref. [57].

For small relative velocities, $vk_{F\downarrow} \ll kT$, it is sufficient to expand the integrand in (12.40) to first order in $\beta\omega_{\mathbf{q}}$. Using the symmetry property $\text{Im}\chi_{\sigma}(q, \omega) = -h\chi_{\sigma}(q, -\omega)$ we obtain

$$\begin{aligned} \frac{d\mathbf{P}\downarrow}{dt} = & -\mathbf{v} \frac{\pi|U|^2}{3kT} \int \frac{d^3q}{(2\pi)^3} q^2 \\ & \times \int_{-\infty}^{\infty} d\omega \frac{\text{Im}\chi_{\downarrow}(q, -\omega)\text{Im}\chi_{\uparrow}(q, \omega)}{(1 - e^{\beta\omega})(1 - e^{-\beta\omega})}. \end{aligned} \quad (12.44)$$

Since $T \ll T_{F\downarrow}$, we can again use the result $\text{Im}\chi_{\sigma}(q, \omega) = m_{\sigma}^* \omega / (4\pi^2 q)$ which yields for the relaxation rate in the limit of low velocities the expression

$$\frac{1}{\tau_P} = \frac{4\pi^3}{9} |\gamma|^2 \frac{m_{\downarrow}^*}{k_{F\uparrow}^2} (kT)^2 = \frac{\pi^3}{9} \frac{1}{\tau_0} \left(\frac{T}{T_{F\downarrow}} \right)^2. \quad (12.45)$$

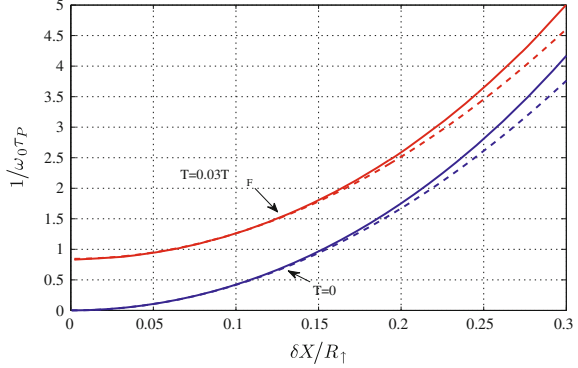
The T^2 -dependence is due to the fact that the phase space for scattering increases with temperature and it is also the same as for a Fermi liquid [55]. Equation (12.45) shows that for equal masses of the two components and at unitarity $1/\tau_P \sim kT^2/T_{F\uparrow}$, as one would expect on dimensional grounds because the effective interaction measured in terms of the density of states of the up-atoms is of the order of unity.

12.5.3 Experimental Consequences for Collective Modes

The previous sections considered the momentum relaxation time for a homogeneous gas. In this section we study the possible consequences on experiments devoted to measure collective mode frequencies in harmonically confined systems. For the sake of concreteness let us analyse the spin dipole mode of a Fermi gas above the critical polarisation where, as previously discussed, the system is normal. We assume that the cloud of minority atoms is displaced by a distance δX from the centre equilibrium position in the harmonic trap. Depending on the amplitude of the displacement (and consequently on the velocity acquired by the minority component due to the external force) as well as on the value of temperature, the cloud either oscillates with weak damping around $\delta X = 0$ (collisionless regime) or it relaxes towards equilibrium without any oscillations (hydrodynamic regime).

In the collisionless limit $\omega_D \tau_P \gg 1$ the dipole mode is well defined and its frequency ω_D can be derived within Landau theory of Fermi liquid (see Sect. 12.6).

Fig. 12.12 The quantity $1/\omega_0\tau_P$ determining the damping of the dipole mode as a function of the amplitude of the oscillation for $T = 0$ and $T = 0.03T_{F\uparrow}$ (For details see text.)



The latter coincides with (12.8) in the extreme imbalance case. The mode becomes over-damped in the hydrodynamic regime $\omega_D\tau_P \ll 1$ since the spin current is not conserved by collisions [58].

In order to estimate $\omega_D\tau_P$ we assume that the displacement of the \downarrow -atom cloud is sufficiently small with respect to the majority cloud size, R_\uparrow , i.e., we consider $\delta X \ll R_\uparrow$, such that the density of \uparrow -atoms may be regarded as uniform when estimating the relaxation rate. Moreover we consider that both component are degenerate and a highly polarised case such that the majority cloud remains essentially at rest during the motion of minority component. The relative velocity of the two components is in this case given by $v = \omega_D\delta X$. Within our assumption we can use the low-speed Eq. 12.42 and low-temperature Eq. 12.45 results which, expressed in terms of the new quantities, read

$$\frac{1}{\omega_0\tau_P} = \frac{81\pi}{25^2} (6N_\uparrow)^{1/3} A^2 \frac{m_\downarrow^*}{m_\uparrow} \left(\frac{T_{F\downarrow}}{T_{F\uparrow}} \right)^2 \left(\frac{\delta X}{R_\uparrow} \right)^2, \quad (12.46)$$

$$\frac{1}{\omega_0\tau_P} = \frac{2\pi^3}{25} (6N_\uparrow)^{1/3} A^2 \frac{m_\downarrow^*}{m_\uparrow} \left(\frac{T}{T_{F\uparrow}} \right)^2, \quad (12.47)$$

respectively, where we have used the result $\gamma = -3/5A$ for a resonant interaction, the fact that $kT_{F\uparrow} = k_{F\uparrow}^2/2m_\uparrow = (6N_\uparrow)^{1/3}\omega_0$ and that ω_D is close to ω_0 .

In Fig. 12.12 we report the full result for the relaxation time of the dipole mode at zero (lower full line) and finite (upper full line) temperature using the values $N_\uparrow = 10^7$, and $N_\downarrow/N_\uparrow = 0.026$ (correspondingly $T_{F\downarrow}/T_{F\uparrow} = 0.3$) which are the conditions achieved in the MIT experiment [9] for a mixture of ${}^6\text{Li}$ -atoms in two different hyperfine states. The lower dashed line is the expression (12.46), while the upper dashed line is the sum of the results (12.46) and (12.47) in the spirit of Landau theory [55]. We see that the analytical results are a good approximation to those obtained by direct numerical integration in the regimes of experimental interest.

The calculated values of $\omega_0\tau_P$ demonstrate that, for the experimental conditions now attainable, the polarised normal phase is easily in a regime intermediate between

collisionless and hydrodynamic behaviour, implying significant damping of the spin dipole mode. At lower temperature, the gas enters the collisionless regime. Indeed such behaviour has been experimentally seen at ENS as reported in [13] (see also Sect. 12.6).

How important collisions are in a given mode is sensitive to the anisotropy of the trap, which we have neglected so far. For instance, cigar-shaped trap ($\omega_z < \omega_\perp$) the transverse mode will be more collisionless, the value of $1/\omega_D \tau_P$ being multiplied by a factor ω_z/ω_\perp for a fixed value of τ_P and by a factor $(\omega_z/\omega_\perp)^{1/3}$, for a fixed value of the trapping frequency geometric average $(\omega_\perp^2 \omega_z)^{1/3}$. When the two atomic species are different, the value of $\omega_0 \tau_P$ will be depend on the trapping potentials of the two species, which can be varied independently of each other.

For low velocity, $m_\downarrow^* v \ll k_{F\downarrow}$, one sees from (12.42) and (12.45) that the momentum relaxation rate scales as m_\downarrow^* . Consequently, since $m_\downarrow^* \approx m_\downarrow$ the spin motion can be made more collisionless by trapping an atom mixture with a lighter minority component. However, calculations indicate that this effect is reduced due to the fact that, at unitarity, the scattering amplitude for the case of extreme imbalance increases with decreasing $m_\downarrow/m_\uparrow < 1$ [23]. For $m_\downarrow/m_\uparrow > 1$ the scattering amplitude is predicted to be approximately constant and therefore $1/\tau_P \propto m_\downarrow$ in this regime. Thus, the spin motion becomes more hydrodynamic for $m_\downarrow/m_\uparrow > 1$.

12.6 Collective Oscillations: The Quadrupole Mode

We have seen that there exists a very good agreement between experiments and the theory developed for the polarised normal phase, when static properties are considered. The theory is essentially based on Landau theory of Fermi liquid, which was built mainly for describing dynamical properties of an interacting Fermi system. Thus a crucial question is whether Landau theory is applicable to the dynamics of strongly interacting normal Fermi gases. In the previous sections we have practically considered only the single particle *out of phase* motion. The aim of the present section is to study the collective mode frequencies of the unitary normal phase as a function of the polarisation. To this purpose we develop the proper Landau formalism to describe the collisionless regime of the polarised Fermi gas.

We face the problem by a lagrangian variational principle to derive the collective modes in the collisionless regime. Such a method has been widely used in nuclear physics to describe collective excitations in an elastic theory of nuclei (see e.g., [59] and reference therein). The variational principle $\delta S = 0$ is applied to the action integral

$$\begin{aligned} S &= \int dt \langle \Psi | H - i \hbar \partial_t | \Psi \rangle \\ &= \int dt (E - \langle \Psi | i \hbar \partial_t | \Psi \rangle), \end{aligned} \quad (12.48)$$

where $|\Psi\rangle$ is a multi-parameter many-body wave-function and $E = \langle\Psi|H|\Psi\rangle$ is the energy functional of the system. The latter on the basis of the Landau-Pomeranchuk energy (12.10) can be written in the form

$$E = \sum_{\sigma} \int d\mathbf{x} \left(\frac{\tau_{\sigma}}{2m} + \frac{m}{2} (\omega_{\perp}^2 r^2 + \omega_z^2 z^2) n_{\sigma} \right) + \frac{3}{5} A \frac{\hbar^2 (6\pi^2)^{2/3}}{2m} \int d\mathbf{x} n_{\downarrow} n_{\uparrow}^{2/3} + a \int d\mathbf{x} \left(\frac{\tau_{\downarrow}}{2m} - \frac{n_{\downarrow}}{2m} \frac{j_{\uparrow}^2}{n_{\uparrow}^2} \right), \quad (12.49)$$

where $\tau_{\sigma}/2m$ is the kinetic energy density of the species σ . The functional (12.49) accounts for the interaction between the majority and the minority component through the local term in A and the last integral, which is necessary in order to keep into account that the polarons (\downarrow -particles) acquires an effective mass due to interaction effects and that galilean invariance implies the presence of a counter current term j_{\uparrow}^2 of the majority component. We include the latter term for completeness, although, since the effective mass is just 10–20% larger than the bare one, the effect of the current term on the frequencies turns out to be fairly small. Expression (12.49) corresponds to a typical energy functional to be used in time-dependent Hartree-Fock approaches in the context of small amplitude and low energy oscillations. It is worth noticing that this approach is equivalent to Landau's theory of Fermi liquid.

At equilibrium the kinetic energy density in Eq. 12.49 reduces to $\tau_{\sigma} = \hbar^2 (6\pi^2 n_{\sigma})^{2/3} n_{\sigma}$ and $j_{\uparrow} = 0$ and, thus, the energy functional Eq. 12.49 can be used to calculate the density profiles using standard variational procedures. The calculation at equilibrium shows that at very high polarization the majority component is scarcely affected by the interaction and, in particular, its radius is in practice given by the ideal gas value

$$R_{\uparrow,i}^0 = (48N_{\uparrow})^{1/6} \sqrt{\frac{\hbar\bar{\omega}}{m\omega_i^2}}, \quad i = x, y, z \quad (12.50)$$

with $\bar{\omega}^3 = \omega_x \omega_y \omega_z$. Instead the radius of the minority component is quenched with respect to the non interacting gas due to the attractive nature of the force. By taking a Thomas-Fermi description for the minority component (which holds with good accuracy for a large class of experimentally available configurations), one finds that the radius of the minority component is given by the simple expression

$$R_{\downarrow}/R_{\uparrow}^0 = \left(\frac{1-P}{1+P} \right)^{1/6} \left(\left(1 + \frac{3}{5} A \right) \frac{m^*}{m} \right)^{-1/4}. \quad (12.51)$$

From Eq. 12.51 it is seen that the minority radius is quite flat as a function of P except at very high polarization when it goes to zero as the inset of Fig. 12.13 shows. We find that this behavior is reflected in the collective mode frequencies.

The proper variational ansatz for the wave function depends on the modes we want to study. We focus on the compressional modes, since the easiest experimental

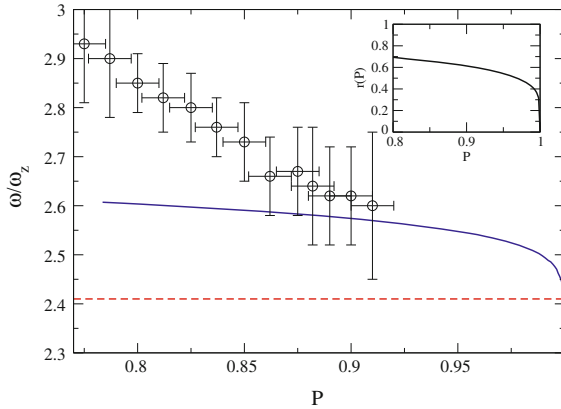


Fig. 12.13 Frequency of the axial compressional mode as a function of the polarization P . *Dashed line*: the single polaron mode frequency. *Solid line*: the collisionless value of the mode frequency obtained via the variational principle described in the present work. Points: experimental data reported in [13]. Inset: the behaviour of the minority radius as a function of P , $r(P) = ((1 - P)/(1 + P))^{1/6}$ (see (12.51))

way of exciting the spin modes in trapped Fermi gases is through a sudden change of the value of scattering length. This procedure, which mainly affects the motion of the impurities, is not able to excite other important oscillations like, e.g., the dipole mode of the minority component and it is the actual procedure employed in the recent experiment reported in Ref. [13]. The starting point are variational single-particle wavefunctions that are then used to build the many-body state as a Slater determinant. In order to study the compressional modes and assuming that the equilibrium configuration is axially symmetric we write the scaling transformation

$$\psi_\sigma(r, z, t) = e^{-1/2(2\alpha_\sigma + \beta_\sigma)} \psi_\sigma^0(e^{-\alpha_\sigma} r, e^{-\beta_\sigma} z) e^{i(\chi_\sigma r^2 + \xi_\sigma z^2)}. \tag{12.52}$$

applied to the single particle wave-functions ψ_σ of the two spin species $\sigma = \uparrow, \downarrow$, and where $r^2 = x^2 + y^2$ and z are the radial and the axial coordinate, respectively. The scaling transformation depends on 4 + 4 time-dependent parameters and the corresponding equations are obtained by imposing the variation $\delta S = 0$ with S as in (12.48) with $\langle \Psi | H | \Psi \rangle$ given by Eq. 12.49. With respect to a typical hydrodynamic energy functional, Eq. 12.49 accounts for the deformation of the Fermi surface produced by the scaling ansatz. This effect arises from the kinetic energy density term τ_σ and exploits the elastic nature exhibited by a Fermi liquid in the collisionless regime. The use of hydrodynamic theory would actually yield wrong predictions for the oscillations of these Fermi gases.

The collective modes are small oscillations around equilibrium, i.e., solutions of the equations of motion derived from the action expanded to second order in the scaling parameters. The first order expansion of the action S with respect to the scaling parameters takes contribution only from the energy functional Eq. 12.49. Then, the

condition $\delta S = 0$ provides a relation between the kinetic and the interaction energy equivalent to the virial theorem. Defining the effective mass as $m/m^* = (1 + a)$ and the averages $N_\sigma \langle f \rangle_\sigma = \int f(r, z) n_\sigma(r, z)$, we obtain

$$\begin{aligned}
& -\frac{4}{3} \int \frac{\tau_\uparrow}{2m} + N_\uparrow m \omega_\perp^2 \langle r^2 \rangle_\uparrow - N_\downarrow \frac{\hbar^2 (6\pi^2)^{2/3}}{2m} A \left(\langle r \partial_r n_\uparrow^{2/3} \rangle_\downarrow + \frac{4}{3} \langle n_\uparrow^{2/3} \rangle_\downarrow \right) = 0, \\
& -\frac{2}{3} \int \frac{\tau_\uparrow}{2m} + N_\uparrow m \omega_z^2 \langle z^2 \rangle_\uparrow - N_\downarrow \frac{\hbar^2 (6\pi^2)^{2/3}}{2m} A \left(\langle z \partial_z n_\uparrow^{2/3} \rangle_\downarrow + \frac{4}{3} \langle n_\uparrow^{2/3} \rangle_\downarrow \right) = 0, \\
& -\frac{4}{3} \int \frac{\tau_\downarrow}{2m^*} + N_\downarrow m \omega_\perp^2 \langle r^2 \rangle_\downarrow + N_\downarrow \frac{\hbar^2 (6\pi^2)^{2/3}}{2m} A \langle r \partial_r n_\uparrow^{2/3} \rangle_\downarrow = 0, \\
& -\frac{2}{3} \int \frac{\tau_\downarrow}{2m^*} + N_\downarrow m \omega_z^2 \langle z^2 \rangle_\downarrow + N_\downarrow \frac{\hbar^2 (6\pi^2)^{2/3}}{2m} A \langle z \partial_z n_\uparrow^{2/3} \rangle_\downarrow = 0,
\end{aligned} \tag{12.53}$$

where all the densities are to be calculated at equilibrium. Note that in the low-concentration or high polarisation limit $N_\downarrow/N_\uparrow \rightarrow 0$ Eq. 12.53 decouples and one recover correctly the result for the free polaron case. Defining $E_{K\sigma}$ the kinetic energy of the σ -component (including the mass m^* for the minority spin- \downarrow component), Eq. 12.53 becomes the standard virial theorem for the majority component

$$-\frac{2}{3} E_{K\uparrow} + N_\uparrow m \omega_\perp^2 \langle r^2 \rangle_\uparrow = 0, \tag{12.54}$$

$$-\frac{1}{3} E_{K\uparrow} + N_\uparrow m \omega_z^2 \langle z^2 \rangle_\uparrow = 0 \tag{12.55}$$

and the virial theorem for a free gas of particles of mass m^* feeling an effective potential for the minority component

$$-\frac{2}{3} E_{K\downarrow} + N_\downarrow m \omega_\perp^2 \left(1 + \frac{3}{5} A \right) \langle r^2 \rangle_\downarrow = 0, \tag{12.56}$$

$$-\frac{1}{3} E_{K\downarrow} + N_\downarrow m \omega_z^2 \left(1 + \frac{3}{5} A \right) \langle z^2 \rangle_\downarrow = 0. \tag{12.57}$$

The term in the action which depends on the time derivative of the wave-function does not give rise to linear terms due to time reversal symmetry. The corresponding quadratic term reads

$$\langle \Psi | i \hbar \partial_t | \Psi \rangle^{(2)} = 2 \sum_\sigma N_\sigma \langle \langle r^2 \rangle_\sigma \alpha_\sigma \dot{\xi}_\sigma + \langle z^2 \rangle_\sigma \beta_\sigma \dot{\chi}_\sigma \rangle. \tag{12.58}$$

Summing up all the contributions and imposing the variational procedure $\delta S = 0$, we get eight coupled equations of motion. Four of them represent continuity equations and are relations between the current parameters ξ_σ , χ_σ and the density ones α_σ , β_σ . In this way we are left to solve a linear system of 4 equations.

We find that the two lowest frequency are almost independent of the ratio N_\downarrow/N_\uparrow and they are very close to the ideal gas values $\omega = 2\omega_\perp$ and $\omega = 2\omega_z$. We call

them the in phase modes since the majority and the minority components move in phase. The frequencies of the other two modes, that we name out of phase or spin modes, can be written as $\omega = 2C_1\omega_\perp$ and $\omega = 2C_2\omega_z$, where the renormalization factors are very close to each other, i.e., $C_1 \simeq C_2$. Such modes correspond to the radial and axial motion of the minority component moving in opposite phase with respect to the majority one. In the limit of a single impurity we recover the value $C_1 = C_2 = \sqrt{(1 + 3/5A)m/m^*}$ of Eq. 12.7.

In Fig. 12.13 we report (solid blue line) the result for the axial spin mode as a function of the polarisation of the system as calculated with the above described variational approach, using for the polaron parameters the values $A = 1.01$ and $m^*/m = 1.17$ [23]. We notice that at high polarisation the correction to the polaron frequency Eq. 12.7, as a function of the polarisation, follows the law $(1 - P)^{1/6}$ characterising the radius of the minority component (see inset in Fig. 12.13 and Eq. 12.51). In Fig. 12.13 we also put the experimental data of [13] and one sees that there is a qualitative difference between the present theory and the experiment [13]. A possible explanation is by invoking the collisional properties of the strongly interacting system even at the lowest achievable temperature as we have discussed in Sect. 12.5. Indeed our prediction was derived in the collisionless regime, while the experiment clearly shows that the in phase mode frequency is strongly affected by collisions even for the highest polarisation available. Understanding the discrepancy between theory and experiment in terms of collisional effects is not however obvious. In fact collisions usually reduce the value of the frequencies with respect to their collisionless values. Thus the question of how the observed frequency in Fig. 12.13 can be compared with our prediction has not an obvious answer.

The Landau theory prediction agrees better with the experimental data at the highest polarisation points, where the collisionless approximation is better satisfied as it can also be inferred from the measurement of the majority component compressional mode frequency reported in [13]. One would then expect that a measurement of the radial compressional mode, would give a much better insight into the problem, since, as we pointed out in Sect. 12.5 for a fixed relaxation time τ , if the radial frequency is much higher than the axial one, the collisions for the radial dipole mode are less effective, being $\omega_\perp\tau \gg \omega_z\tau$. As a last comment, we should remind that the energy functional (12.49) is strictly valid only at high polarization, being an expansion in the concentration n_\downarrow/n_\uparrow . It works however quite well when applied to investigate the static properties even till the critical concentration. For instance the inclusion of the next term proportional to $(n_\downarrow/n_\uparrow)^2$ introduces only small corrections to the values of the radii, even close to the critical polarization limit $P_C = 0.77$. Thus one can think that such a term does not change the picture previously described.

Acknowledgments We are indebted to F. Chevy, S. Giorgini, C. Pethick, L. P. Pitaevskii, C. Salomon, W. Zwerger and M. Zwierlein for very useful discussions. We acknowledge support by EuroQUAM Fermix program and by MIUR PRIN 2007.

References

1. Inguscio, M., Ketterle, W., Salomon, C.: Ultracold Fermi Gases. In: Proceedings of the International School of Physics "Enrico Fermi", Course CLXIV, Varenna (2006)
2. Giorgini, S., Pitaevskii, L., Stringari, S.: *Rev. Mod. Phys.* **80**, 1215 (2008)
3. Bloch, I., Dalibard, J., Zwirger, W.: *Rev. Mod. Phys.* **80**, 885 (2008)
4. Leggett, A.J.: *J. Phys. C* **41**, 7 (1980)
5. Nozieres, P., Schmitt-Rink, S.: *J. Low Temp. Phys.* **59**, 195 (1985)
6. Chandrasekhar, B. S.: *Appl. Phys. Lett.* **1**, 7 (1962)
7. Clogston, A. M.: *Phys. Rev. Lett.* **9**, 266 (1962)
8. Zwierlein, M.W., Schirotzek, A., Schunck, C.H., Ketterle, W.: *Science* **311**, 492 (2006)
9. Shin, Y., Zwierlein, M.W., Schunck, C.H., Schirotzek, A., Ketterle, W.: *Phys. Rev. Lett.* **97**, 030401 (2006)
10. Shin, Y., Schunck, C.H., Schirotzek, A., Ketterle, W.: *Nature* **451**, 689 (2008)
11. Partridge, G.B., Li, W., Kamar, R.I., Liao, Y.A., Hulet, R.G.: *Science* **311**, 503 (2006)
12. Partridge, G.B., Li, W., Liao, Y.A., Hulet, R.G., Haque, M., Stoof, H.T.C.: *Phys. Rev. Lett.* **97**, 190407 (2006)
13. Nascimbene, S., Navon, N., Jiang, K.J., Tarruell, L., Teichmann, M., McKeever, J., Chevy, F., Salomon, C.: *Phys. Rev. Lett.* **103**, 170402 (2009)
14. Nascimbene, S., Navon, N., Jiang, K., Chevy, F., Salomon, C.: *Nature* **463**, 1057 (2010)
15. Navon, N., Nascimbene, S., Chevy, F., Salomon, C.: *Science* **328**, 5979 (2010)
16. Lobo, C., Recati, A., Giorgini, S., Stringari, S.: *Phys. Rev. Lett.* **97**, 200403 (2006)
17. Schirotzek, A., Wu, C.-H., Sommer, A., Zwierlein, M. W.: *Phys. Rev. Lett.* **102**, 230402 (2009). Online supplemental material at <http://prl.aps.org/supplemental/PRL/v102/i23/e230402>
18. Mahan, G.D.: *Many-Particle Physics*. Kluwer Academic, Dordrecht (2000)
19. Prokofev, N.V.: *Phys. Rev. Lett.* **74**, 2748 (1995) (and references therein)
20. Arias de Saavedra, F., Boronat, J., Polls, A., Fabrocini, A.: *Phys. Rev. B* **50**, 4248 (1994) (and references therein)
21. Lifshitz, E.M., Pitaevskii, L.P.: *Statistical Physics Part 2*. Pergamon Press, New York (1980)
22. Chevy, F.: *Phys. Rev. A* **74**, 063628 (2006)
23. Combescot, R., Recati, A., Lobo, C., Chevy, F.: *Phys. Rev. Lett.* **98**, 180402 (2007)
24. Pines, D.: *The Many-Body Problem*. W. A. Benjamin Inc, New York (1962)
25. Combescot, R., Giraud, S., Leyronas, X.: *Eur. Phys. Lett.* **88**, 60007 (2009)
26. Mora, C., Chevy, F.: *Phys. Rev. A* **80**, 033607 (2009)
27. Punk, M., Dumitrescu, P.T., Zwirger, W.: *Phys. Rev. A* **80**, 053605 (2009)
28. Prokof'ev, N., Svistunov, B.: *Phys. Rev. B* **77**, 020408 (2008)
29. Pilati, S., Giorgini, S.: *Phys. Rev. Lett.* **100**, 030401 (2008)
30. Combescot, R., Giraud, S.: *Phys. Rev. Lett.* **101**, 050404 (2008)
31. Giraud, S., Combescot, R.: *Phys. Rev. A* **79**, 043615 (2009)
32. McGuire, J.B.: *J. Math. Phys. (N.Y.)* **7**, 123 (1966)
33. Lipparini, E.: *Modern many-particle physics: atomic gases, nanostructures and quantum liquids*, 2nd edn. World Scientific Publishing Company, Singapore (2008)
34. Recati, A., Lobo, C., Stringari, S.: *Phys. Rev. A* **78**, 023633 (2008)
35. Mora, C., Chevy, V.: *Phys. Rev. Lett.* **104**, 230402 (2010)
36. Yu, Z., Zöllner, S., Pethick, C. J.: <http://arxiv.org/abs/1006.4723>
37. Carlson, J., Chang, S.Y., Pandharipande, V.R., Schmidt, K.E.: *Phys. Rev. Lett.* **91**, 050401 (2003)
38. Astrakharchik, G.E., Boronat, J., Casulleras, J., Giorgini, S.: *Phys. Rev. Lett.* **93**, 200404 (2004)
39. Haussmann, R., Rantner, W., Cerrito, S., Zwirger, W.: *Phys. Rev. A* **75**, 023610 (2007)
40. Bausmerth, I., Recati, A., Stringari, S.: *Phys. Rev. Lett.* **100**, 070401 (2008)
41. Bausmerth, I., Recati, A., Stringari, S.: *Phys. Rev. A* **78**, 063603 (2008)
42. Urban, M., Schuck, P.: *Phys. Rev. A* **78**, 011601(R) (2008)

43. The fact that the results obtained at RICE [10,11] showed the presence of a superfluid at any value of the polarization, i.e., of h , is still quite puzzling.
44. Bracewell, R.N.: *The Fourier Transform and Its Applications*. McGraw-Hill, New York (1986)
45. Wille, E. et al.: *Phys. Rev. Lett.* **100**, 053201 (2008)
46. Taglieber, M., Voigt, A.-C., Aoki, T., Hänsch, T.W., Dieckmann, K.: *Phys. Rev. Lett.* **100**, 010401 (2008)
47. Bausmerth, I., Recati, A., Stringari, S.: *Phys. Rev. A* **79**, 043622 (2009)
48. Fumi, F.G.: *Phil. Mag.* **46**, 1007 (1955)
49. Wu, S.-T., Pao, C.-H., Yip, S.-K.: *Phys. Rev. B* **74**, 224504 (2006)
50. Pao, C.-H., Wu, S.-T., Yip, S.-K.: *Phys. Rev. A* **76**, 053621 (2007)
51. Parish, M.M., Marchetti, F.M., Lamacraft, A., Simmons, B.D.: *Phys. Rev. Lett.* **98**, 160402 (2007)
52. Ketterle, W., Zwierlein, M.: In: Inguscio, M., Ketterle, W., Salomon, C. (eds.) *Proceedings of the International School of Physics Enrico Fermi, Course CLXIV*, p. 95. IOS Press, Amsterdam (2008)
53. Punk, M., Zwerger, W.: *Phys. Rev. Lett.* **99**, 170404 (2007)
54. Schneider, W., Shenoy, V. B., Randeria, M.: <http://arxiv.org/abs/0903.3006>
55. Pines, D., Nozières, P.: *Theory of Quantum Liquids Volume I: Normal Fermi Liquids*. W. A. Benjamin, New York (1966)
56. Baym, G., Pethick, C.J.: *Landau Fermi-liquid Theory: Concepts and Applications*. Wiley, New York (1991)
57. Bruun, G., Recati, A., Pethick, C., Smith, H., Stringari, S.: *Phys. Rev. Lett.* **100**, 240406 (2008)
58. Vichi, L., Stringari, S.: *Phys. Rev. A* **60**, 4734 (1999)
59. Stringari, S.: *Ann. Phys.* **151**, 35 (1983)